Click Here for Full Article

Coupling of mass transfer and reactive transport for nonlinear reactions in heterogeneous media

M. Willmann,[1,2] J. Carrera,[3] X. Sanchez-Vila,[2] O. Silva,[3] and M. Dentz[3]

Received 16 January 2009; revised 9 February 2010; accepted 26 February 2010; published 14 July 2010.

[1] Fast chemical reactions are driven by mixing-induced chemical disequilibrium. Mixing is poorly represented by the advection-dispersion equation. Instead, effective dynamics models, such as multirate mass transfer (MRMT), have been successful in reproducing observed field-scale transport, notably, breakthrough curves (BTCs) of conservative solutes. The objective of this work is to test whether such effective models, derived from conservative transport observations, can be used to describe effective multicomponent reactive transport in heterogeneous media. We use a localized formulation of the MRMT model that allows us to solve general reactive transport problems. We test this formulation on a simple three-species mineral precipitation problem at equilibrium. We first simulate the spatial and temporal distribution of mineral precipitation rates in synthetic hydraulically heterogeneous aquifers. We then compare these reaction rates to those corresponding to an equivalent (i.e., same conservative BTC) homogenized medium with transport characterized by a nonlocal in time equation involving a memory function. We find an excellent agreement between the two models in terms of cumulative precipitated mass for a broad range of generally stationary heterogeneity structures. These results indicate that mass transfer models can be considered to represent quite accurately the large-scale effective dynamics of mixing controlled reactive transport at least for the cases tested here, where individual transport paths sample the full range of heterogeneities represented by the BTC.

Citation: Willmann, M., J. Carrera, X. Sanchez-Vila, O. Silva, and M. Dentz (2010), Coupling of mass transfer and reactive transport for nonlinear reactions in heterogeneous media, *Water Resour. Res.*, *46*, W07512, doi:10.1029/2009WR007739.

1. Introduction

[2] Understanding and modeling multicomponent reactive transport at the field scale is a necessary condition for the design of remediation strategies in groundwater pollution problems and for risk assessment evaluations. Numerical and analytical methods are available to address multicomponent reactive transport problems at the local scale. Yet, it is not clear whether they can be extended to the field scale. Aquifers are heterogeneous at all scales with hydraulic conductivity values spanning over orders of magnitude, even in seemingly homogeneous aquifers. As a result, large scale transport in spatially heterogeneous media is different from the transport observed in homogeneous media and in general non-Fickian. Realistic hydrogeological applications must directly or indirectly embed this heterogeneity.

[3] Under certain conditions [e.g., *Dagan*, 1989; *Gelhar*, 1993], asymptotic large scale transport of conservative species can be described by the advection-dispersion equation (ADE) with upscaled transport parameters. The asymptotic limit is typically given by the time after which the species distribution is spread out over a volume whose dimensions are much larger than the largest heterogeneity scale. At preasymptotic times, however, which are relevant for most hydrogeological problems, observations [e.g., *Adams and Gelhar*, 1992] display what is known as anomalous (non-Fickian) or nonergodic [*Kitanidis*, 1988] behavior, so that concentrations are not well simulated by an ADE, even allowing for upscaled parameters [*Carrera*, 1993]. In fact, *Neuman* [1990] proposes an universal scaling law stating that aquifers display an evolving range of scales and, therefore, nonergodic conditions apply to all transport problems, regardless of travel distance.

[4] At the other end, departures from Fickian behavior are also frequently observed at the laboratory scale [*Valocchi*, 1985; *Levy and Berkowitz*, 2003]. To describe effective transport of conservative species at intermediate distances different nonlocal methods have been developed: continuous time random walks (CTRW) [*Berkowitz and Scher*, 1998; *Berkowitz et al.*, 2006], fractional advection-dispersion equations (fADE) [*Benson et al.*, 2000], multirate mass transfer (MRMT) [*Haggerty and Gorelick*, 1995; *Silva et al.*, 2009], and memory functions [*Carrera et al.*, 1998]. The last two methods are mathematically equivalent. Furthermore, it has been shown [*Dentz and Berkowitz*, 2003; *Berkowitz et al.*, 2006] that fADE and MRMT can be formulated as CTRWs. Recent reviews and comparisons of nonlocal methods can be found in work by, e.g., *Berkowitz et al.* [2006], *Neuman and Tartakovsky* [2009], and *Silva et al.* [2009].

[1]Institute of Environmental Engineering, ETH Zurich, Zurich, Switzerland.
[2]Department of Geotechnical Engineering and Geosciences, Technical University of Catalonia, Barcelona, Spain.
[3]Institute of Environmental Assessment and Water Research, CSIC, Barcelona, Spain.

Copyright 2010 by the American Geophysical Union.
0043-1397/10/2009WR007739

[5] All these nonlocal methods are suited for describing non-Fickian BTCs of field and laboratory experiments [*Berkowitz and Scher*, 1998; *Kosakowski et al.*, 2001; *McKenna et al.*, 2001; *Levy and Berkowitz*, 2003; *Haggerty et al.*, 2004; *Cortis and Berkowitz*, 2004; *Zinn et al.*, 2004; *Le Borgne and Gouze*, 2008] and thus give valuable insight into the mechanisms of anomalous transport behavior in heterogeneous aquifers [*Schumer et al.*, 2003; *Dentz and Berkowitz*, 2003; *Berkowitz et al.*, 2006; *Zhang et al.*, 2007; *Berkowitz et al.*, 2008; *Willmann et al.*, 2008].

[6] The question is whether nonlocal formulations for representing conservative transport can be extended to reactive transport. Since reactive transport is very sensitive to the nature of reactions [*Rubin*, 1983], the fact that a certain effective description works for one type of reaction does not imply that it works for others. That is, we need to define the type of reactions to be addressed. Reactions can be classified as linear or nonlinear, as controlled by kinetics (slow) or equilibrium (fast), as homogeneous (all reactants in the same phase) or heterogeneous, etc. Transport of sorptive species in heterogeneous media was investigated with emphasis on the spatial or the temporal distribution of concentrations since the early works of *Selroos and Cvetkovic* [1992] and *Bellin et al.* [1993]. In fact, MRMT was initially developed as a way to model heterogeneous sorption problems, and has been widely used in this context [*Roth and Jury*, 1993; *Rubin et al.*, 1997; *Haggerty and Gorelick*, 1998; *Lawrence et al.*, 2002; *Berkowitz et al.*, 2008]. Recently, *Dentz and Castro* [2009] and *Dentz and Berkowitz* [2005] demonstrated that transport under spatially heterogeneous linear equilibrium adsorption properties, is effectively represented by CTRW, or, equivalently, by MRMT.

[7] Regarding equilibrium or kinetic reactions, the situation is more complex. It can be shown [e.g., *Margolin et al.*, 2003] that effective transport in heterogeneous media under linear kinetic reactions occurring homogeneously throughout the domain can be represented by the same nonlocal model as conservative solutes because the overall reaction rate is controlled by the residence time distribution, which is precisely what the BTC represents. Therefore, any model that reproduces the BTC for a conservative solute also reproduces the BTC and the overall reaction rate for solutes undergoing linear reactions. This is not necessarily the case for multicomponent equilibrium or nonlinear kinetic reactions. *Rezaei et al.* [2005] and *De Simoni et al.* [2005, 2007] showed that equilibrium reaction rates are controlled by mixing and depend on the species concentrations in a nonlinear way.

[8] The nonlocal formulations described above reproduce conservative BTCs, that is solute arrival times, but not necessarily mixing. In fact, one can fit a given BTC with models that consist of independent flow tubes with virtually no mixing [*Medina and Carrera*, 1996; *Luo and Cirpka*, 2008]. The handling of mixing is precisely what distinguishes the ADE and the nonlocal formulations presented before. The ADE equates spreading and mixing, both quantified by macroscale hydrodynamic dispersion coefficients. At preasymptotic times, such a transport description overestimates solute mixing and rather quantifies the rate of growth of the area that could potentially be affected by a pollutant [e.g., *Dentz et al.*, 2000; *Dentz and Carrera*, 2007].

[9] Mixing describes the rate at which two water bodies blend [e.g., *Kitanidis*, 1994; *Kapoor and Kitanidis*, 1998; *De Simoni et al.*, 2005]. *Cirpka and Kitanidis* [2000] showed for moderately heterogeneous fields that transverse dispersion controls mixing. At the local scale, transverse dispersion results from the interplay between molecular diffusion and velocity fluctuations caused by heterogeneity. Molecular diffusion is the actual trigger mechanism for mixing as it is the only process that mixes solute between independent paths lines [e.g., *Dentz and Carrera*, 2007; *Zavala-Sanchez et al.*, 2009]. As the molecular diffusion is almost constant, advective heterogeneity seems to control mixing already at the Darcy scale. Therefore, to study the effect of heterogeneity on mixing it is important to use a strong physical heterogeneity and a smaller transverse dispersion in order not to blend two different sources of advective heterogeneity. Since mixing controls many chemical reactions it is clear that mixing should be accounted for in the governing equations for multicomponent reactive transport in heterogeneous media.

[10] Work on the effect of heterogeneity on integrated reaction rates under equilibrium conditions has been limited. *Luo et al.* [2008], *Binning and Celia* [2008], *Cirpka et al.* [2008], and *Fernandez-Garcia et al.* [2008] evaluated the global reaction rate for either generally heterogeneous or stratified media, concluding that the integrated reaction rate could not be obtained from an upscaled ADE equation. *Lichtner and Kang* [2007] used a lattice-Boltzmann model to simulate pore scale precipitation/dissolution. Their model is effectively equivalent to a MRMT model, but does not address the effect of hydraulic heterogeneity.

[11] The objective of this work is, thus, to investigate whether a mass transfer model is an appropriate tool to describe mixing controlled multicomponent reactive transport in heterogeneous aquifers. Our goal is to test whether upscaling of conservative transport is sufficient to upscale reactive transport. For this purpose we propose a model that couples the MRMT model with reactions. We then compare the results in terms of the spatial and temporal distribution of instantaneous reaction rate and cumulative reaction, between detailed heterogeneous simulations in synthetic aquifers using the ADE, and those coming from the MRMT model with the known memory function derived from conservative transport.

2. Multirate Mass Transfer Reactive (MRMT-R) Model

[12] In this section we propose a model for multicomponent reactive transport that extends the general MRMT model. This is done in three steps, starting with the corresponding model for conservative solute, presented here for completeness, then showing the local scale reactive problem we consider in this paper (mixing induced precipitation), and finally coupling the two models to derive the MRMT-R model.

2.1. Conservative Transport Model Based on Multirate Mass Transfer

[13] Amongst the different effective models available in the literature to represent transport in heterogeneous media, we select one based on multirate mass transfer, for reasons that will become apparent when extending it to account for reactions. The MRMT model represents the system as composed by a mobile and a suite of immobile regions that coexist at any given point in the domain. These regions

SCIPEDIA
Register for free at https://www.scipedia.com to download the version without the watermark

interact. Solute mass is transferred between the mobile and each of the immobile regions proportional to the difference in the concentrations. This linear exchange can be seen as diffusion. In fact, the model was originally developed to represent diffusion into actual immobile regions. The underlying idea is that flow paths with varying velocities (residence times) coexist at some elementary volume, and solute is transferred between paths by local diffusion/dispersion. The MRMT model is an obvious simplification of reality. However, it provides sufficient degrees of freedom to accommodate any residence time distribution and, indeed, it can be used to fit BTCs measured in lab or field tracer tests [e.g., *McKenna et al.*, 2001; *Haggerty et al.*, 2004].

[14] The MRMT model considers a governing equation which involves an advective, a dispersive and a sink/source term to account for mass transfer with immobile zones. Therefore, the resulting equation for concentration of a conservative species j in the mobile zone, $c_{m,j}$, can be written as

$$\phi_m \frac{\partial c_{m,j}}{\partial t} = \nabla \cdot (\mathbf{D} \nabla c_{m,j}) - \mathbf{q} \cdot \nabla c_{m,j} - \Gamma_j \tag{1}$$

where $\mathbf{D}$ is the dispersion tensor, ϕ_m is the porosity corresponding to the mobile zone, i.e., the ratio between pores accessible by advection and the total volume, and Γ_j is the source/sink term controlling the mass transfer of species j between the mobile and the suite of immobile regions, which we write as [*Carrera et al.*, 1998; *Haggerty et al.*, 2000]

$$\Gamma_j = \phi_{i_{tot}} \left[g^* \frac{\partial c_{m,j}}{\partial t} + g c_{m0,j} \right] \tag{2}$$

where $c_{m0,j}$ is the initial concentration of the jth species, $*$ indicates a convolution (in time), product, and $\phi_{i_{tot}}$ is the total immobile porosity, defined as the void volume fraction that is not accessible by advection. With this definition, the actual porosity (measurable in the field) is just $\phi = \phi_m + \phi_{i_{tot}}$. Function g, termed memory function, accounts for the probability distribution of the time that a solute particle remains in the immobile regions. In general, this function will depend on the velocity distribution.

[15] Equations (1) and (2) are termed "nonlocal" in time because they do not depend only on $c_{m,j}(x, t)$, but also on the past history of concentrations. In order to incorporate reactions in an efficient way, we seek a formulation of (1) that involves only the local species concentrations at a given point and time, that is, we seek a 'local' formulation of the above nonlocal transport problem. To this end, we expand the memory function as a sum of exponentials

$$g(t) = \sum_{i=1}^{N} \alpha_i b_i e^{-\alpha_i t} \tag{3}$$

where α_i is the inverse of the characteristic waiting time associated to the ith term, and b_i is the corresponding fraction of the immobile porosity. Notice that this expansion is equivalent to discretizing the residence time distribution. More interesting, it is equivalent to viewing the immobile region as consisting of N immobile regions, each of which exchanges mass with rate α_i [*Carrera et al.*, 1998; *Haggerty et al.*, 2000]:

$$\frac{\partial c_{im,j,i}}{\partial t} = \alpha_i (c_{m,j} - c_{im,j,i}) \tag{4}$$

where $c_{im,j,i}$ denotes concentration of species j in the immobile zone i. Combining (3) and (4) allows, after some algebra, rewriting (2) as (see Appendix B for details)

$$\Gamma_j = \sum_{i=1}^{N} \alpha_i \phi_i (c_{m,j} - c_{im,j,i}) \tag{5}$$

where $\phi_i = b_i \phi_{i_{tot}}$ is the immobile porosity associated to exchange rate α_i (or residence time $1/\alpha_i$). Imposing

$$\sum_{i=1}^{N} \phi_i = \phi_{itot} \tag{6}$$

is equivalent to having $\sum_{i=1}^{N} b_i = 1$.

[16] In principle a large suite of memory functions could be used. The main feature of these functions is their behavior at large times, since they control the late time behavior of breakthrough curves [*Haggerty et al.*, 2000]. Also, in principle a large number of parameters should be fitted (actually $2N - 1$). For this reason, the memory function is parameterized by a small number of parameters [e.g., *Rubin et al.*, 1997; *Carrera et al.*, 1998; *Lawrence et al.*, 2002; *Haggerty et al.*, 2000] in most applications. Amongst these, a commonly used model is the truncated power law [e.g., *Dentz et al.*, 2004], where function $g(t)$ can be expressed in terms of two characteristic times, t_1 (time at which the power law behavior starts manifesting), t_2 (time at which concentration starts departing faster than the power law), and the slope of the memory function, m_g.

2.2. Reactive Transport in a Single-Porosity Model

[17] The model presented in the previous subsection accounts for a conservative solute undergoing advection, dispersion at the local scale and mass transfer between mobile and less mobile (mathematically treated as immobile) zones. In this section we extend the model to incorporate a binary precipitation-dissolution reaction at equilibrium, but it could be extended to any system involving $p \geq 2$ aqueous species with $q \geq 1$ equilibrium reactions, along the lines of *De Simoni et al.* [2005]. The binary system proposed involves two reacting aqueous species, B_j, $j = 1, 2$ (their respective aqueous concentrations being $c_{m,1}$ and $c_{m,2}$, in chemical equilibrium with a mineral S at any point in space and time:

$$B_1 + B_2 \longleftrightarrow S \tag{7}$$

[18] The concentrations of the aqueous species are nonlinearly related by means of the mass action law, which, under the assumption of low ionic strength can be written as

$$c_{m,1} \cdot c_{m,2} = K \tag{8}$$

where K is the equilibrium constant, modified for the activity coefficients. Therefore, K will be a function of local

SCIPEDIA
Register for free at https://www.scipedia.com to download the version without the watermark

chemistry and temperature. Without loss of generality, and for the sake of simplicity, we disregard this variability. The equality in equation (8) implies that the mineral is widely available at all points in space. The governing nonlinear transport equations for the two aqueous species become

$$\phi_m \frac{\partial c_{m,j}}{\partial t} = \nabla \cdot (\mathbf{D} \nabla c_{m,j}) - \mathbf{q} \cdot \nabla c_{m,j} - r_m \qquad j = 1, 2 \tag{9}$$

where r_m is the reaction rate, defined as the amount of precipitated moles per unit volume of aquifer and unit of time. Note, that in equation (9) we keep the subindex m in the concentrations and the reaction rate to indicate that they correspond to that of the mobile zone; this identification will be useful in the sequel. Note also that, since r_m is the same for $j = 1$ and 2, it is possible to define a linear combination of the concentrations (denoted as component):

$$u_m = c_{m,1} - c_{m,2} \tag{10}$$

so that the chemical source term r_m is eliminated and the governing equation is that of a conservative quantity:

$$\phi_m \frac{\partial u_m}{\partial t} = \nabla \cdot (\mathbf{D} \nabla u_m) - \mathbf{q} \cdot \nabla u_m \tag{11}$$

[19] A more general reactive transport problem involving p aqueous species with q equilibrium reactions could be defined in terms of $p - q$ components. The component definition in equation (10) is not unique. Another conservative quantity would also be obtained by multiplying equation (10) by a scalar. The resulting transport equation (equation (11)) is independent of r_m because precipitation removes the same amount of moles of the two species. Therefore, their difference is unaffected by reaction (which is the definition of conservative quantity). Assuming that it is possible to obtain a solution for the component u_m, the two concentrations can be obtained explicitly by solving the speciation problem (i.e., solving equations (8) and (10))

$$c_{m,1} = \frac{u_m}{2} + \sqrt{\frac{u_m^2}{4} + K} \qquad c_{m,2} = -\frac{u_m}{2} + \sqrt{\frac{u_m^2}{4} + K} \tag{12}$$

[20] In many applications the main quantity of interest is the reaction rate, rather than the actual solute concentrations. This would be the case, e.g., in natural attenuation studies, karst formation, mineral precipitation, etc. The reaction rate can then be obtained from equation (9). Alternatively, *De Simoni et al.* [2005] derived an explicit expression for the calculation of r directly from the solution of the component, being the product of two terms, one of them depending only on speciation r_{spec} and a second one which depends on the concentration gradients and the dispersion tensor and characterizes mixing r_{mix}

$$r = r_{spec} r_{mix} \tag{13}$$

with

$$r_{spec} = \frac{\mathrm{d}^2 c_{m,2}}{\mathrm{d}u_m^2} = \frac{2K}{(u_m^2 + 4K)^{3/2}} \qquad r_{mix} = \nabla^T u_m \mathbf{D} \nabla u_m \tag{14}$$

2.3. Multirate Mass Transfer Reactive (MRMT-R) Model

[21] Combining the two models presented in this section, it is possible to incorporate nonlinear reactions into the MRMT model. An important point to note here is that the incorporation of "immobile regions" in our effective model is just a mathematical artifact to account for the amount of solute that samples the less mobile parts of the domain. For this reason, sink terms should be included in the "immobile zones" to account for the precipitation that takes place when the solutes reaching those areas by diffusion (actually slow advection) generate chemical disequilibrium with the mineral. It is important to state that we can have a different chemical equilibrium condition in each one of the zones (mobile plus N immobile). Thus, even though we preserve chemical equilibrium at all points, defining concentration by averaging over scales larger than the pore, effectively it appears that equilibrium is not preserved [*Luo et al.*, 2008; *Binning and Celia*, 2008; *Donado et al.*, 2009]. This issue has significant implication for total reaction rates, which will be explored later.

[22] Combining equations (9) and (1), and introducing (5) we can write the governing equation for the MRMT-R model

$$\phi_m \frac{\partial c_{m,j}}{\partial t} = \nabla \cdot (\mathbf{D} \nabla c_{m,j}) - \mathbf{q} \cdot \nabla c_{m,j} - \sum_{i=1}^{N} \alpha_i \phi_i (c_{m,j} - c_{im,j,i}) - r_m \qquad j = 1, 2 \tag{15}$$

The mass balance for the ith immobile zone is written as an extension of (4)

$$\phi_i \frac{\partial c_{im,j,i}}{\partial t} = \phi_i \alpha_i (c_{m,j} - c_{im,j,i}) - r_{im,i} \qquad j = 1, 2 \tag{16}$$

where $r_{im,i}$ is the mass removed (by precipitation) per unit volume of aquifer and unit of time in the immobile zone i. Introducing equation (10), the equations satisfied by the conservative component read

$$\phi_m \frac{\partial u_m}{\partial t} = \nabla \cdot (\mathbf{D} \nabla u_m) - \mathbf{q} \cdot \nabla u_m - \sum_{i=1}^{N} \alpha_i \phi_i (u_m - u_{im,i}) \tag{17}$$

$$\frac{\partial u_{im,i}}{\partial t} = \alpha_i (u_m - u_{im,i}) \tag{18}$$

where we have introduced $u_{im,i} = c_{im,1,i} - c_{im,2,i}$. Provided we have a way to solve equations (17) and (18) component in terms of u_m and $u_{im,i}$, the actual concentration values in the mobile zone are given by equation (12) plus

$$c_{im,1,i} = \frac{u_{im,i}}{2} + \sqrt{\frac{u_{im,i}^2}{4} + K} \qquad c_{im,2,i} = -\frac{u_{im,i}}{2} + \sqrt{\frac{u_{im,i}^2}{4} + K} \tag{19}$$

Finally the reaction rates can be obtained as

$$r = r_m + \sum_{i=1}^{N} r_{im,i} \tag{20}$$

SCIPEDIA
Register for free at https://www.scipedia.com to download the version without the watermark

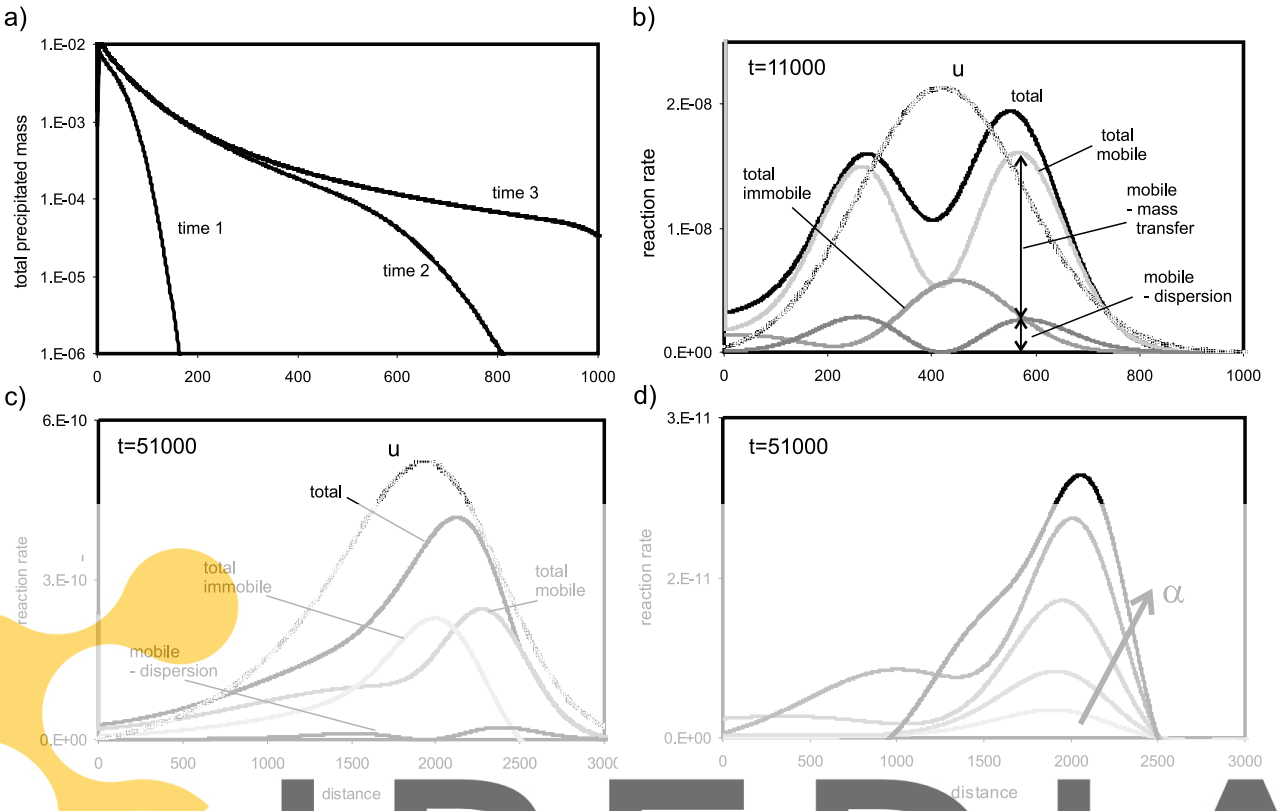

Figure 1. Evaluation of the spatial distribution of mineral precipitation. (a) Total precipitated mass for three different times (1000, 11000, 51000). (b) Spatial distribution of reaction rate for an early time step (t only slightly larger than t_1); reaction rate in the mobile zones shows some ADE like behavior with the characteristic double peak and is much stronger than reaction rate in the immobile zone. (c) The same plot for a later time step, where no double peaks are displayed anymore (notice the different horizontal scale in the plots). (d) Distribution of selected single immobile zones for the same time as Figure 1c; the total number of immobile zones is 20.

SCIPEDIA
Register for free at https://www.scipedia.com to download the version without the watermark

with r_m obtained from equation (15), and $r_{im,i}$ being after equation (16)

$$r_{im,i} = -\phi_i \frac{\partial c_{im,j,i}}{\partial t} - \phi_i \alpha_i (c_{im,j,i} - c_{m,j}) \qquad (21)$$

where the value of $r_{im,i}$ is independent of j, that is, of the species used for computing the mass balance. It is important to note that the impact of heterogeneity is comprised only in the memory function, which is determined from conservative transport. An alternative expression to equation (21) can be found in work by *Donado et al.* [2009]. Some insights into the numerical implementation of MRMT-R are given in Appendix A.

3. Behavior of the MRMT-R Model

[23] The MRMT-R model discussed in section 2 depends on a number of parameters, including those that define the memory function, mobile and immobile porosity, and the equilibrium constant, among others. In this section we explore the behavior of the model by analyzing the 1-D problem discussed by *Willmann et al.* [2008].

[24] The domain is 3000 elements units long. A hydraulic gradient is imposed so that water flows in the positive x direction with a flux of 0.0062 (in consistent units). Mobile porosity, ϕ_m, equals 0.147 and the longitudinal dispersivity, α_l, 33.8, all in consistent units. The immobile regions are characterized by an immobile porosity, $\phi_{i_{tot}}$, of 0.153 (total porosity is 0.3) and a following memory function with: slope, m_g, of 1 and characteristic times t_1, t_2, of 8000 and 800000 (all reported times are in consistent units). The memory function is discretized using 20 terms with the α and b distributions of *Willmann et al.* [2008]. Initial water displays a constant chemical signature represented by $u_m = u_{im,i} = 0$, equivalent to consider that the concentrations of the two species are identical $c_{m,1} = c_{m,2} = c_{im,1,i} = c_{im,2,i}$ $(\forall i)$. During a short interval at the beginning ($\Delta t = 1000$) a pulse of $u = c_1 - c_2 = 0.5$ is applied at the inlet boundary. That is, water with a different chemical composition, but still in chemical equilibrium with the mineral, enters the domain. After this time interval, the system is flushed by water with the initial composition ($u = 0$). In this particular simple geochemical setup whenever two end-member waters (the initial one and that entering the system) are in equilibrium with the mineral, any of their mixtures will be oversaturated. Therefore, precipitation takes places wherever mixing occurs.

[25] Results are displayed in Figure 1. Notice that for t = 11000 (only slightly larger than t_1), diffusion into immobile regions has barely started acting as the mass transfer mechanism and the conservative component concentration in the

mobile region looks quite Gaussian. In fact, the peak is located at $x \simeq 420$, when it should have been located at $x = qt/\phi_m = 443$, if transport had been restricted to the mobile region. On the other hand, the conservative component u displays a marked tailing and a slight retardation (peak at 1900, while advection through the mobile region would have brought it to 2130) at $t = 51000$, when diffusion into immobile regions has become relevant. The behavior of the solution in terms of reaction rates is discussed below.

3.1. Spatial Distribution of Reaction Rate in the Mobile and Immobile Zones

[26] Due to the specified boundary conditions, the largest amount of precipitation takes place at the inlet (left) boundary (Figure 1a). With time reactions extend along the flow path. Overall mineral precipitation in our model is the sum of that taking place in the mobile and in the N immobile zones (equation (20)). At early times the spatial distribution of reaction rates in the mobile zone resembles what would be obtained from an ADE transport model, with a characteristic symmetric double peak and a zero value in between (the actual expression given by equation (14)). The double peak is still present in the MRMT-R model, but the minimum value is no longer zero, and the leading peak is slightly larger than the trailing peak (the shape is nonsymmetrical; see Figure 1b). The relatively large reaction rate obtained in the mobile region reflects the two mixing mechanisms present in equation (15), i.e., dispersion and exchange with immobile regions. The total r_m is obtained from mass balance in equation (15). The reaction rate caused by dispersion is calculated using equation (13) rate and the rest is caused by exchange with immobile regions. Both for small and for large times, mixing (and consequently reaction) due to mass transfer is much larger than that due to dispersion (Figures 1b and 1c). This is particularly relevant at small times considering that dispersion is typically viewed as affecting the qualitative shape of the conservative component.

[27] For small times, the total reaction rate integrated over all immobile zones is much smaller than that at the mobile zone, and displays a single maximum located in between the two peaks of mobile zone reaction rate (slightly ahead of the u peak). For later times, the total reaction rate distribution displays a single peak (Figure 1c). Now, mobile and immobile reaction rates display similar shapes, with their maxima shifted toward the front, and long trailing tails. The peak corresponding to the immobile zone is slightly delayed with respect to that of the mobile one. Individual reaction rates for 5 zones out of the total $N = 20$ are shown in Figure 1d. The reaction rate for each individual zone appears to be double humped. The first hump corresponds to the mass transfer into the immobile zone. It is the largest and slightly lagged with respect to the plume peak, with the lag time decreasing with increasing mass transfer coefficient α. The second hump corresponds to the mass transfer out of the immobile zone. It is also delayed inversely proportional to α. In fact, the two humps nearly overlay for very large α values. The model is not very sensitive to the amount of immobile zones used. Results were visually identical when the number of zones was reduced from 20 to 10. Differences became noticeable when the number of zones was further reduced to 5.

[28] Simulation of mixing in this model is subtle. On the one hand, reaction at the mobile zone caused by mass exchange with the mobile region resembles mixing caused by dispersion. On the other hand, reaction caused by mixing within the immobile regions is quite proportional to the difference between mobile and immobile concentrations. The implication is that, contrary to what might be expected, mass transfer with immobile regions does not necessarily imply full mixing between initial and inflowing waters. Little actual mixing occurs for zones whose characteristic time ($1/\alpha$) is small compared to the concentration rise. That is, these zones are effectively in equilibrium with the mobile region. And they act as if their water was replaced rather than mixed (i.e. their effect is equivalent to an increase in mobile porosity and dispersivity). On the other hand, zones with much larger characteristic times (small α) do act as fully delayed mixing causing tailing for point injections and delaying reaction for continuous injection. The implication of this discussion is that, although mixing and spreading are not equated in the MRMT-R model, they are not quite independent either. Mobile and immobile regions contribute to both.

3.2. Sensitivity to the Equilibrium Constant

[29] Reaction rates at the local scale can be expressed as the product of two independent terms: the mixing factor and the speciation factor (e.g., equation (13) rate). While our work focuses on mixing, the speciation factor may also be important and is discussed here briefly to facilitate understanding of later results. In our geochemical setup the speciation factor is controlled entirely by the values of equilibrium constant, K, and the component u. Figure 2a illustrates the dependence of the speciation factor on u for several K values. For large u, the speciation factor is largest for large K, but the opposite holds for low K. Moreover, for small values ($u \leq \sqrt{K}$) the speciation factor is virtually constant, but drops as $u^{-3/2}$ for large u values.

[30] Nonmonotonic dependence of the speciation factor with respect to K translates to the quantification of overall precipitation (Figure 2b). Together with the nonlinearity of the mixing factor, it leads to a somewhat unpredictable behavior of reaction rates. The spatial distribution of precipitation rate changes dramatically with K. The reference case discussed before used $pK = -log_{10}(K) = 2$. When K is decreased ($pK = 4$) the overall behavior changes slightly. The reaction rate is generally increased and a slight double peak is developed. For $pK = 6$ this effect is much more pronounced and we see a well developed double peak. The reason here is not, as in the previous section, incomplete mixing within the immobile zone but that the reaction hardly takes place at peak concentrations but only at much lower ones.

4. MRMT-R Upscaling Methodology

[31] *Willmann et al.* [2008] showed that a MRMT model could be used to provide an effective picture of conservative transport through heterogeneous media. They analyzed how the memory function is affected by different parameters characterizing the heterogeneity of the system, such as the variance of log hydraulic conductivity. The main objective in this section is to find whether and under which conditions, the MRMT-R model is capable of reproducing key features of multicomponent reactive transport in heterogeneous media where an ADE is assumed at the local scale. The working

SCIPEDIA
Register for free at https://www.scipedia.com to download the version without the watermark

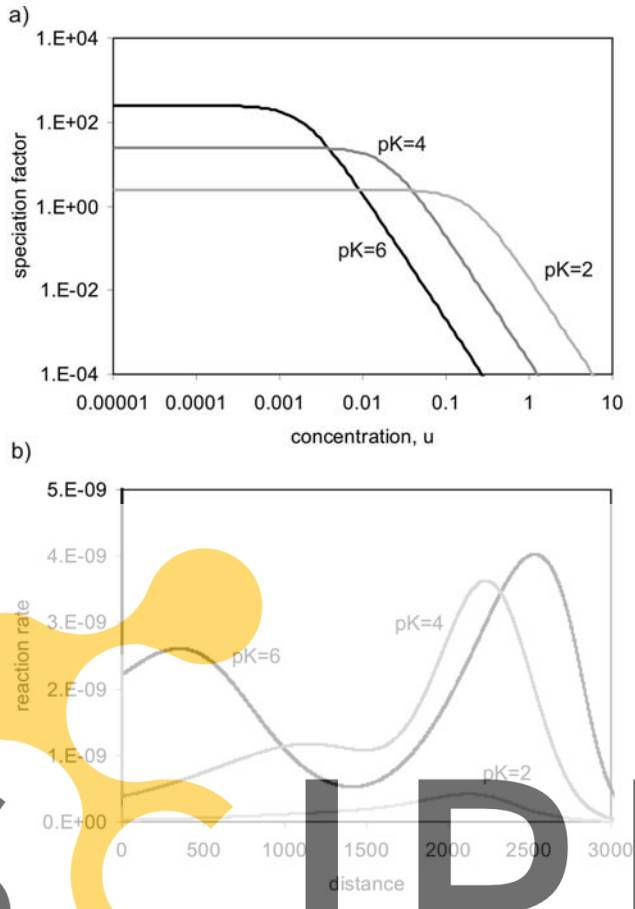

Figure 2. (a) Speciation factor (equation (14)) as a function of concentration for different pK ($-log_{10}K$) values. The speciation factor increases with pK for low values of u, but decreases for high values). (b) Spatial distribution of the reaction rate (equation (15) rate) for $t = 51000$ in the example of Figure 1 for the three values of K. The reaction rates are nonmonotonic with K.

SCIPEDIA
Register for free at https://www.scipedia.com to download the version without the watermark

hypothesis is that the memory function that is derived from conservative transport would be directly applicable to reactive transport. This is why our 2D heterogeneous fields represent individual (hydro)geological units with strong internal heterogeneities rather than complex large scale areas with different units with possibly individually different memory functions.

[32] The methodology we use is numerical and can be summarized in the following steps: (1) we create heterogeneous transmissivity fields with some characteristic features; (2) we perform reactive transport simulations in the heterogeneous fields based on a local description of transport governed by an ADE equation with a single sink/source term to account for precipitation/dissolution; (3) we derive a memory function from the BTCs observed for a conservative species; (4) we model reactive transport in a homogenized media by using the MRMT-R model with the memory function derived from the conservative transport, and (5) we test whether the MRMT-R simulations actually match the observed curves in the heterogeneous media. These steps are explained next.

4.1. Generation of Heterogeneous Transmissivity Fields

[33] We conceptualize the aquifer as two dimensional. We focus on transport at intermediate distances compared to a larger characteristic heterogeneity scale (such as the correlation distance whenever it exists), where power law tails are frequently observed in the field. According to *Willmann et al.* [2008] tailing occurs due to the presence of connected regions of high conductivity (preferential flow paths). For this reason we use individual realizations of heterogeneous fields obtained as follows (the actual selected fields can be seen in Figure 3). The first field studied is an individual unconditional realization of a multi-Gaussian field with a small correlation length (λ = 20 in consistent units). This field was generated using the Gaussian sequential simulator GCOSIM3D [*Gómez-Hernández and Journel*, 1993]. This first field is used for comparison, since transport in multi-Gaussian fields has been the topic of extensive research. The second field corresponds to an individual realization of a conditional simulation using a power variogram. The conditioning points (not shown in Figure 3) are selected to produce a single preferential flow path connecting the high permeability pixels. By construction, this field exhibits an evolving range of scales. The third field is a connected field constructed using the methodology of *Knudby and Carrera* [2006]. This results in a field with narrow high T paths surrounded by low conductive regions. The variance of log transmissivity (Y) is set to 6 in all three fields. The exponential covariance model was used in all three cases. Still, this does not limit our results as model predictions are insensitive to the choice of the covariance model as long as uncertainties are not considered [*Riva and Willmann*, 2009]. The domain size is 1024 by 512 elements of unit size. No flow is imposed on top and bottom and constant head boundaries on the remaining sides, forcing a mean uniform flow from left to right. The overall gradient is 0.0098. Notice that we are interested in looking at the characteristics of transport in individual realizations, and this is the reason not to pursue a Monte Carlo approach.

4.2. Reactive Transport Simulations

[34] Local scale reactive transport in the heterogeneous fields is assumed to be described by the ADE. Note that the basic methodology can easily be extended to a different form of the local transport equation. We focus on local scale advective-dispersive transport because we are mainly interested in the loss of information in the upscaling process. We used the approach outlined in section 2.2. That is, we first solved transport of a conservative component (equation (11)) followed by speciation (equation (12)). The initial condition is $u_m = u_{im,i} = 0$.

[35] Boundary conditions are similar to those explained in the previous section but imposed in all boundary nodes corresponding to the 2D domain. That is, a pulse of $u = 0.5$ is applied to the water entering through the left nodes during a short interval at the beginning (Δt = 1000). This is followed by flushing with $u = 0$ water (initial conditions). The remaining parameters for the local scale equation are a porosity of 0.3 and longitudinal and transverse dispersivities of 10 and 1, respectively. Molecular diffusion is not explicitly modeled. While molecular diffusion triggers mixing at the pore scale, its effect overcome by mechanical dispersion at the Darcy scale. Concentrations are computed from

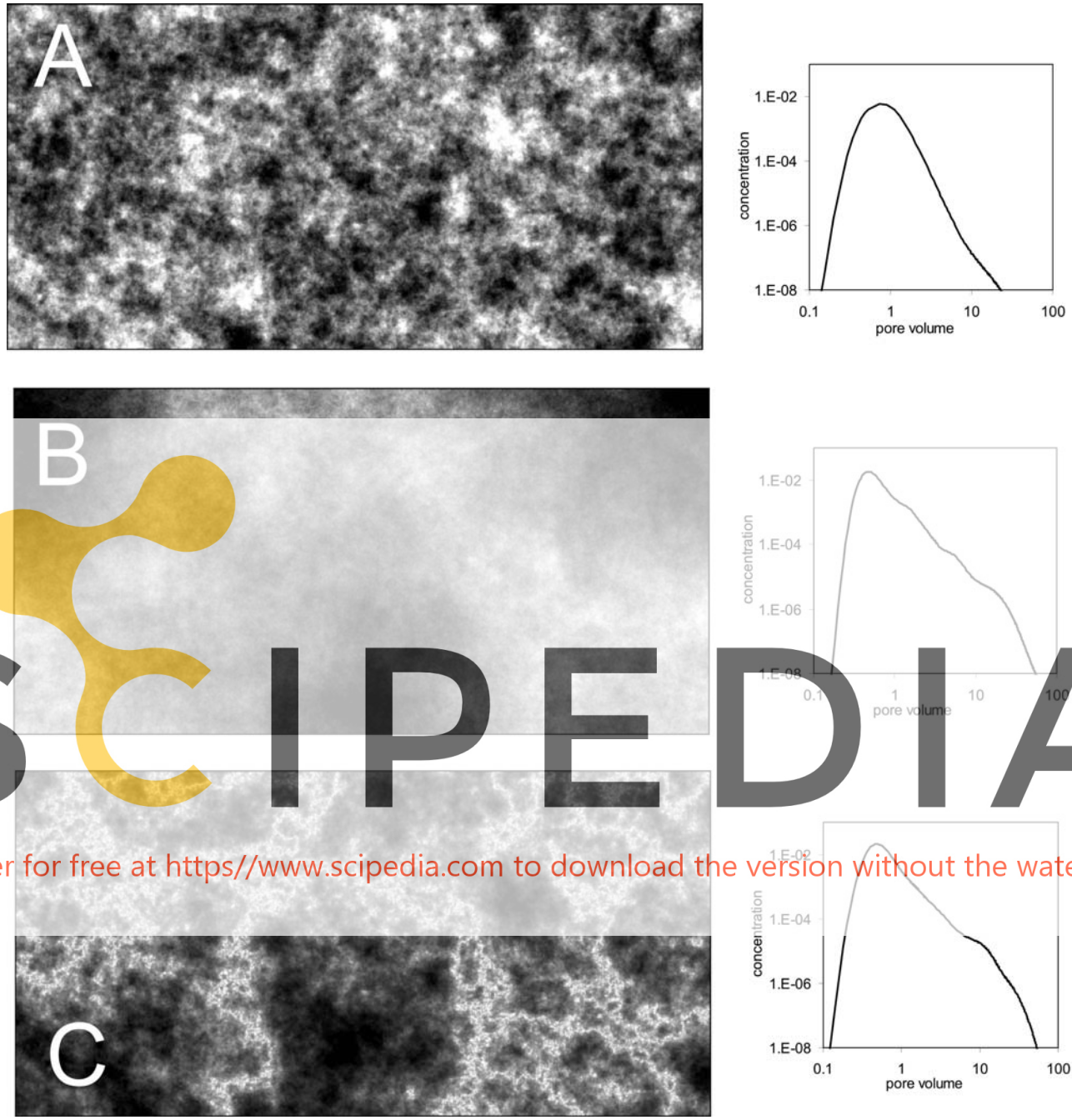

SCIPEDIA
Register for free at https//www.scipedia.com to download the version without the watermark

Figure 3. Transmissivity fields and corresponding breakthrough curves (BTCs) obtained from conservative transport simulations. BTCs are the cumulated mass collected at the domain's right boundary. The three fields correspond respectively to single realizations of (a) a multi-Gaussian field with short correlation length, (b) a nonstationary field based on a power variogram, and (c) a field where connectivity between the high transmissive pixels have been enhanced with respect to those of low conductivity.

equation (12). The reaction rate is calculated at each time step and each node through mass balance, that is solving for r_m in equation (9), and the cumulative precipitated mass is recorded. Simulations are performed using code FAITH [*Sánchez-Vila et al.*, 1993], which solves the transport equation using the Galerkin finite element method. The algorithm is only conditionally stable, which restricts the values of dispersivity we can use. But it is highly accurate, which ensures that no numerical dispersion is present. Figure 4 shows an example plot of total precipitated mass. One clearly sees "hot spots" of strong precipitation at locations where strong mixing takes place. Analysis of Figure 4 is nontrivial. Some hot spots occur at zones of fast transport, where flow tubes become very narrow, so that local transverse dispersion becomes a very efficient mixing mechanism [*Werth et al.*, 2006]. However, zones of fast transport downstream of other hot spots display moderate precipitation because reactive capacity has been exhausted.

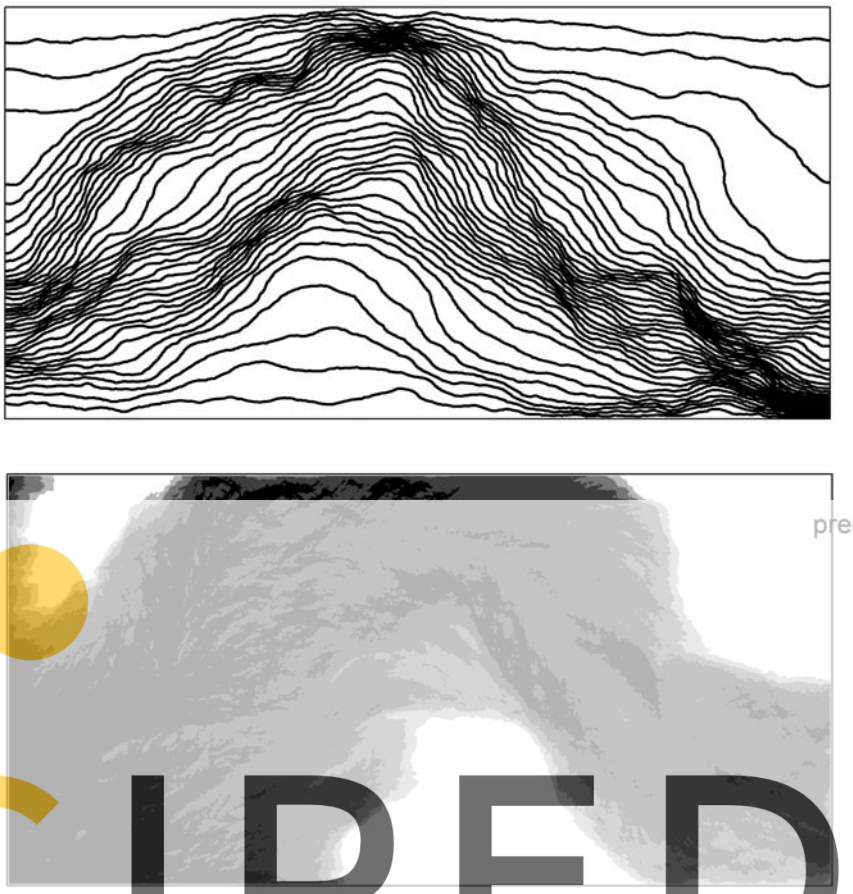

Figure 4. (top) The flow field and (bottom) the spatial distribution of total precipitated mass for a Type B field. One can see hot spots (dark) of large precipitation where more mixing occurs. The flow lines generally appear to become narrower in these areas [*Werth et al.*, 2006]. It supports our hypothesis that the flow fields and, therefore, heterogeneity controls mixing in such a highly heterogeneous field.

SCIPEDIA
Register for free at https//www.scipedia.com to download the version without the watermark

4.3. Derivation of Memory Function for Conservative Transport

[36] The three BTCs presented in Figure 3, corresponding to a conservative species, can be represented using an MRMT model with a memory function derived according to *Willmann et al.* [2008]. From a given BTC, one derives an upscaled value for longitudinal dispersivity and mobile porosity from the early time arrival of the BTC. The three parameters defining the memory function are taken from late time behavior. The two characteristic times when the power law behavior starts, t_1, and ends, t_2, and the slope of the BTC, m_{BTC}. The slope of the memory function, m_g, is related to the slope of the BTC and depends on the boundary condition. The two slopes are identical for resident concentration, while for flux-averaged concentration $m_g = m_{BTC} - 1$. The last relevant parameter in the model, the immobile porosity, calculated by $\phi_{i_{tot}} = \phi_{tot} - \phi_m$, so as to ensure that total porosity remains unchanged.

5. Effective Reactive Transport Behavior

[37] Type A field shows an almost Fickian behavior with a slightly noticeable tail (Figure 3). The curves recorded from the Type B and C fields show anomalous (non-Fickian) behavior. While these two fields are very different in terms of their internal structure, they render similar breakthrough curves, so that the fitted memory functions are almost identical. The next step is to analyze how reactive transport behaves in these fields and compare the results to those obtained from the equivalent model. The comparison is done in terms of vertically averaged spatial distributions of (1) instantaneous reaction rates, and (2) cumulative precipitated mass. In the following we study the effective reactive transport behavior for heterogeneous fields, which cause non-Fickian effective conservative transport (Type B and C), and fields, for which effective conservative transport is essentially Fickian (Type A).

5.1. Non-Fickian Conservative Transport

[38] Looking at fields B and C, we find clear indicators of anomalous conservative transport. The breakthrough curves for conservative solutes display the peak well ahead of one pore volume and a power law late time behavior. This behavior can be reproduced using a MRMT model.

[39] Field C is characterized by thin channels within a matrix of less conductive material. Figure 5a shows a very good match in terms of cumulative precipitated mass versus distance for three selected time steps when comparing the results from the real (heterogeneous) 2D field and the upscaled 1D mass transfer model. The remarkable point is that both the spatial distribution and the time evolution are well reproduced. This observation is independent of the value

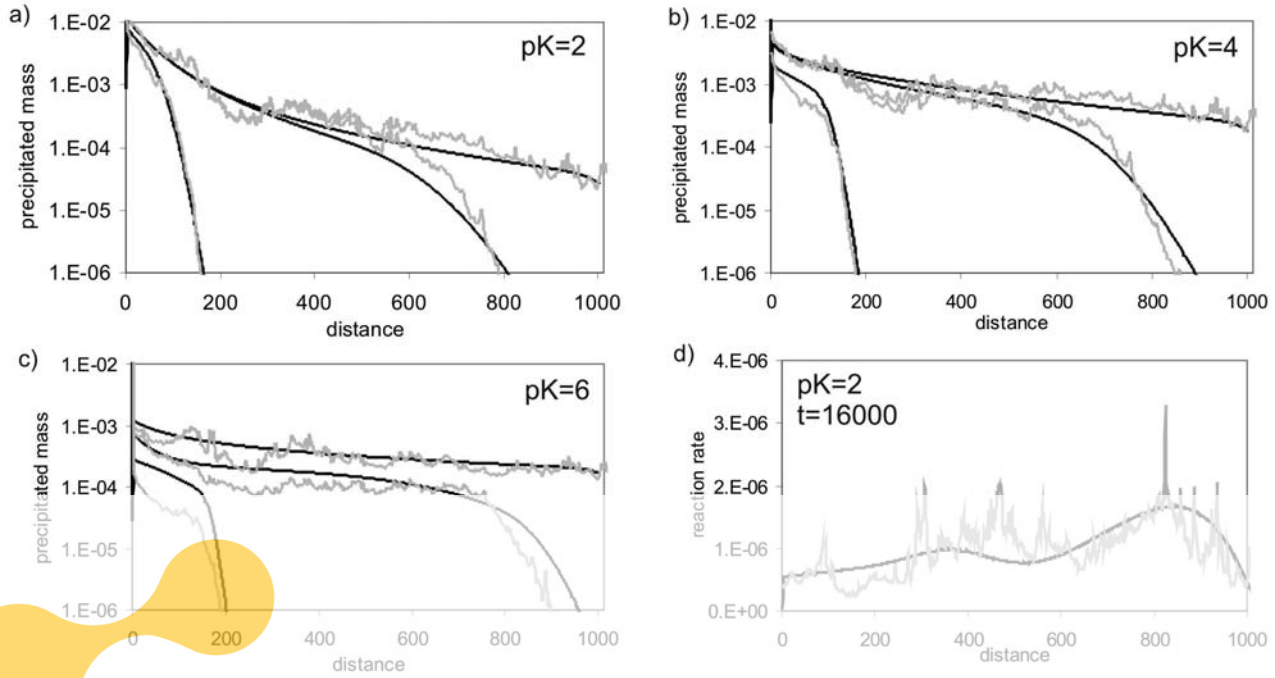

Figure 5. Model results for field type C (connected field). Comparison between the spatial distributions of the vertically averaged precipitated mass in the heterogeneous media with those derived from the effective MRMT-R model for three different time steps (1000, 11000, 51000) and for (a) pK = 2, (b) pK = 4, and (c) pK = 6. (d) The instantaneous reaction rate for both models at a given time step for pK = 2, showing a good agreement in the instantaneous spatial distribution.

SCIPEDIA
Register for free at https://www.scipedia.com to download the version without the watermark

of the equilibrium constant K (Figures 5b and 5c), despite the very nonlinear response to this particular parameter: larger K values (=0.01) lead to larger precipitation close to the outlet, while smaller K values provide a similar amount of precipitate throughout the system for late times.

[40] The spatial distribution of vertically averaged reaction rates at one time step for the type C field is shown in Figure 5d. The heterogeneous curve displays a slight double peak with the largest peak at the front. This behavior is reproduced quite well with the mass transfer model. Already at such early time the effective model is capable of reproducing the main features of the heterogeneous solution. We also compared the reaction rate at later times (not shown), but as most of the mass has left the domain only the tails were fitted.

[41] Type B field (Figure 3) is characterized by large scale structures, and the transitions from high to low conductive zones are more gradual than in the Type C field. Still, memory functions in those two fields are almost identical. Figure 6 displays the comparison of precipitated mass versus distance for some specific times and different K values. The agreement is still quite remarkable. On the contrary, when comparing now the spatial distribution of instantaneous reaction rate in both models (see Figure 6d) the match is rather poor. The heterogeneous medium leads to a double peaked curve, with the two peaks of similar size, while the effective model provides a hardly noticeable second peak, and a long backwards tail. In this case the fluctuations in vertically integrated reaction rates are sensitive to the presence of very large low and high conductive zones (Figure 3). This effect is averaged out when integrated in the BTC across the full domain. At larger travel times (not shown) the agreement improves slightly. Still, we must conclude that the methodology does not ensure good reproduction of local reaction rates, which is to be expected because an upscaling approach does not need to reproduce local scale effects. Instead, large scale trends should be simulated. In fact, the spatial distribution of cumulative reactions rates is qualitatively reproduced in all cases and times analyzed.

5.2. Quasi-Fickian Conservative Transport

[42] Ergodic transport will eventually develop whenever travel distance is much larger than the correlation length along the mean flow direction. In such a case transport can be described by means of an ADE characterized by the mean flow velocity and a constant macrodispersion coefficient. This is the reason we incorporated field A in our simulations. The conservative BTC at the outlet boundary shows a close to Fickian behavior (recall Figure 3). The heterogeneous reactive transport results are shown in Figure 7. In Figure 7a we also show the difference between considering an ADE, with an upscaled dispersivity coefficient of 85.0, or a MRMT model with mobile and immobile porosities and dispersivity equal to 0.2, 0.1 and 45.0, respectively, and the memory function characterized by a slope of 2.0 and characteristic times of $t_1 = 6 \times 10^2$ and $t_2 = 9 \times 10^5$. For large enough travel times, the spatial distributions of cumulative precipitate in the two models are practically identical except at the leading front. Generally, our model agrees quite well with heterogeneous solution except at the outlet, which is affected by the boundary condition. However, again the spatial distribution of the reaction rate, Figure 7b, is not well reproduced by the effective quasi-Gaussian model indicating that the local mixing mechanisms are not well captured by the

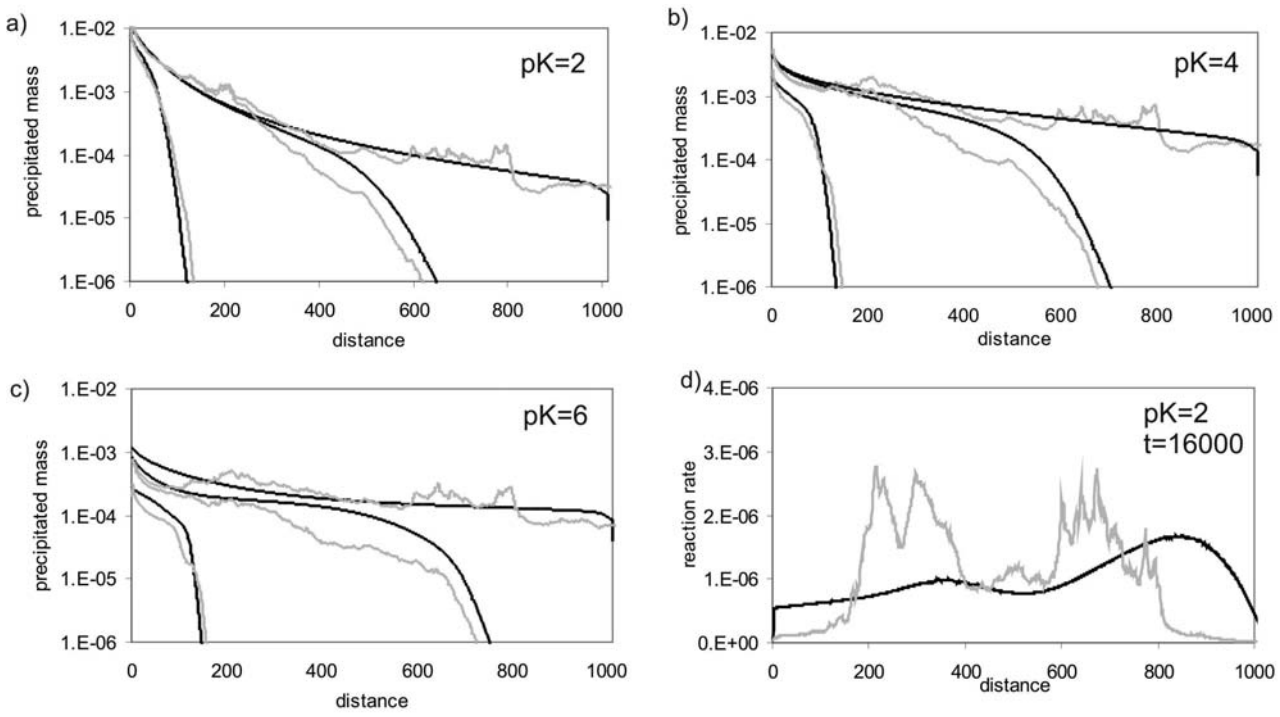

Figure 6. Model results for field type B (nonstationary variogram). Comparison between the spatial distributions of the vertically averaged precipitated mass in the heterogeneous media with those derived from the effective MRMT-R model for three different time steps (1000, 11000, 51000) and for (a) pK = 2, (b) pK = 4, and (c) pK = 6. (d) The instantaneous reaction rate for both models at a given time step for pK = 2.

effective quasi-Gaussian model. Similar behavior has been observed by *Luo et al.* [2008].

6. Sensitivity Analysis

[43] In this section, we study the sensitivity of the observed effective reactive transport behavior to the applied initial and boundary conditions and, more, importantly, to the value of transverse dispersivity, which is usually viewed as the key parameter in reactive transport modeling.

6.1. Initial and Boundary Conditions

[44] The slope of a BTC depends strongly on the initial and boundary condition applied. Yet, the memory function does not change [*Haggerty et al.*, 2000]. In all previous simulations an initial pulse proportional to flux is applied at the inlet boundary of the heterogeneous field. This results in a flux-averaged boundary condition, leading to a BTC slope of m_{pulse}. Applying a uniform initial distribution leads to a different BTC, with a slope m_{unif}. *Willmann et al.* [2008] found that whenever the boundary itself samples all the variability of the system, $m_{unif} = m_{pulse} - 1$. We look now at the implications for reactive transport. Figure 8 displays the spatial distributions of precipitated mass for these two boundary conditions on Field C. We adjust the duration of the pulse input ($t_p = 610$) and the number of columns where constant concentration are initially present (13) to assure the same mass of solute enters in the system in both simulations. Far from the inlet boundary the overall precipitation is larger for the flux-averaged boundary case than for the initial uniform pulse. The opposite happens close to the boundary. This difference in mass precipitated is caused by the dominant transport mechanism in this field being flow within the fast flowing channels, so that the largest amount of precipitation takes place along the channels. The homogeneously distributed case seems to have only 1/5 of the mass within these channels compared to the reference case. The MRMT-R model using the same memory function accounts very well for both solutions with respect to total precipitated mass. Intuitively one expects resident concentration to be used in reactive transport, particularly as reactions takes place also where water is almost stagnant (immobile zone). But from our simulations we conclude that the distinction between flux concentration and resident concentration only depend of the boundary condition of the problem and that MRMT-R is capable of properly accounting for both.

6.2. Transverse Dispersion

[45] Transverse dispersion, α_T, and molecular diffusion are particularly important for reactive transport as they are the main local scale parameters that control mixing [*Cirpka and Kitanidis*, 2000]. Here, we compare the distributions of precipitated mass for three different α_T values for the heterogeneous reference field C (Figure 8b). It can be seen that the total precipitated mass is only slightly affected by the choice of the α_T value. The larger the value, the smoother the curve, but the actual values do not change much. It can also be seen that a larger transverse dispersion value delays the precipitation for earlier time steps. In fact, this behavior also occurs for conservative transport. It reflects the delayed arrival of the mixing front caused by larger α_T. For comparison the effective mass transfer model is shown as well and it can be observed that all three α_Ts are represented well with the

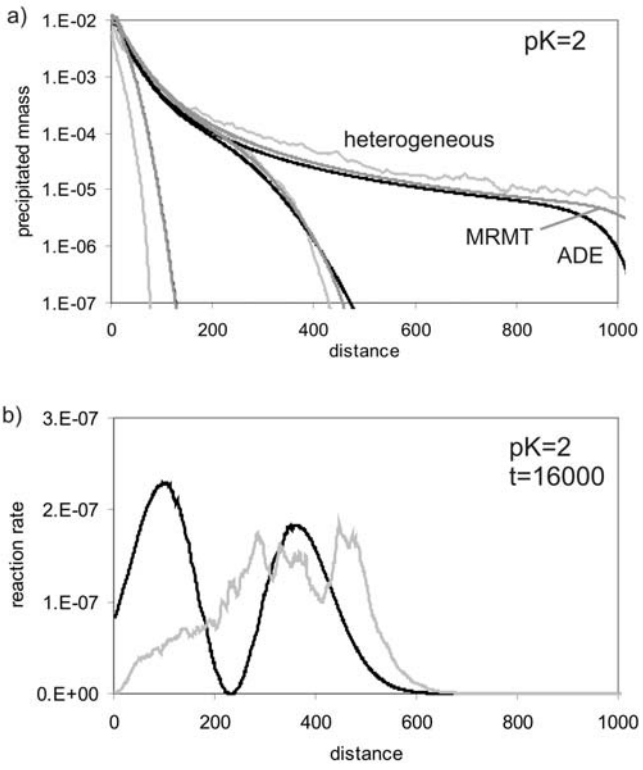

Figure 7. Model results for field type A. (a) Comparison between the spatial distribution of the vertically averaged precipitated mass in the heterogeneous media with those derived from the effective MRMT-R model for three different time steps (1000, 11000, 51000) and for pK = 2. (b) The instantaneous reaction rate for both models at a given time step.

MRMT-R model, which by construction does not take into account α_T.

[46] Our results show that α_T has little effect on the distribution of the precipitated mass. This is somewhat puzzling, because transverse dispersion has been assumed to control mixing. We conclude that α_T while being the controlling factor describing local scale mixing and, thus, a necessary trigger for reactive transport, seems to be of subleading importance for the quantification of the precipitated mass in strongly heterogeneous fields. This apparent paradox can be attributed to the fact that large scale mixing is controlled here by explicit heterogeneity. Local scale dispersion at the Darcy scale, or molecular diffusion at the pore scale, are needed as a trigger mechanism, but the actual rate of large scale mixing and reaction are determined by heterogeneity. This is an important prerequisite for upscaling procedure of mixing as the upscaled parameters only account for mixing lost through homogenization and not as well for the one lost through reduction of dimension.

7. Conclusions

[47] We present an effective reactive mass transfer model and investigate whether this model based on upscaling of conservative transport is sufficient to upscale mixing controlled multicomponent reactive transport. We develop a mass transfer model (MRMT-R) for a binary precipitation dissolution system which is based on an upscaled memory function derived from the observed BTC of a conservative solute. Generally, we find that the MRMT-R model is an excellent tool for representing mixing controlled reactive transport. In particular:

[48] 1. Total precipitation is well reproduced for all the examples studied, in terms of both the total mass precipitated and its spatial distribution for short, intermediate and large travel times.

[49] 2. The MRMT-R model mathematically separates reactions taking place in the mobile and immobile zones. The distinction is to some extent arbitrary. Fast flowing parts of the domain can be modeled either within the mobile porosity with an upscaled dispersion or within the immobile porosity with large exchange rates, leading to practically identical spatial distributions of overall reaction rates.

[50] 3. Applying different initial and boundary conditions changes the reactive transport behavior dramatically. A uniform initial (resident) distribution leads to stronger precipitation close to the inlet boundary and less precipitation

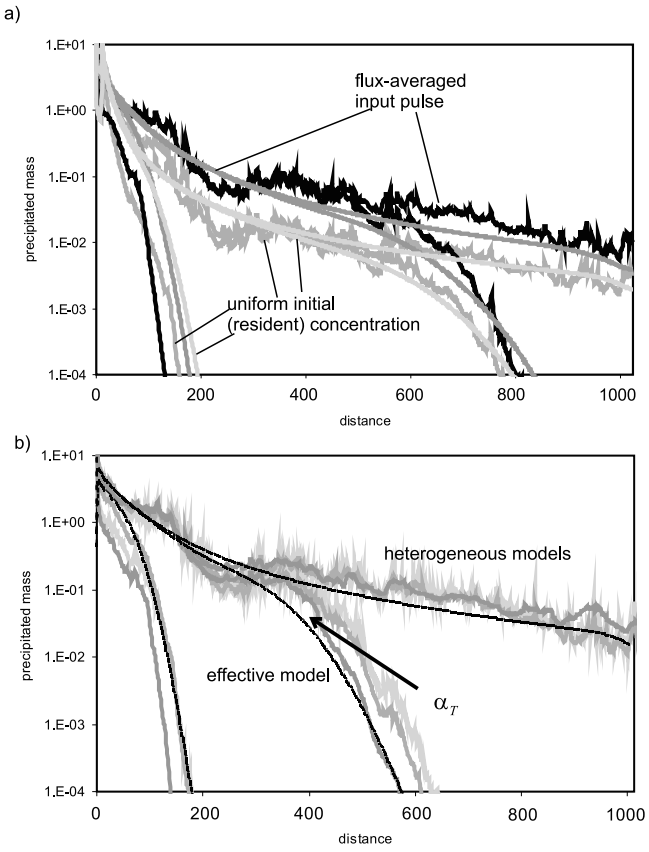

Figure 8. Sensitivity analysis for (a) boundary conditions, including an flux averaged input pulse and initial uniform concentration at the boundary nodes. After a distance of 200 the curves have the same shape but the precipitated mass when a pulse is considered is 5 times larger than for fixed initial concentration. The smoother cures are the effective MRMT-R models which both reproduce very well the heterogeneous solution. (b) Transverse dispersivities (0.1, 1.0, 10.0) is varied. The curves look similar but smooth out with increasing dispersivity. The corresponding effective solution represents very well all the heterogeneous curves.

further downstream when compared to a flux weighted input. Interestingly, the spatial distribution for the two cases further away form the boundary is more or less the same with lower values for the uniform initial distribution. The MRMT-R model reproduces very well precipitation for either boundary condition using the same memory function.

[51] 4. Local scale mixing parameters (transverse dispersivity and molecular diffusion) have only a minor effect on total precipitation for the large scales investigated here, but they need to be present as a trigger mechanism to obtain reactions. For larger scales mixing appears to be controlled by advective heterogeneity described by a conservative memory function. The larger the transverse dispersivity, the smoother the curve. That transverse dispersion is not very important for large scale reactive transport is critical as MRMT-R (and most of the existing upscaled models) does not explicitly account for it. Molecular diffusion was not modeled explicitly, even it is a conceptual prerequisite for local scale mixing. This limits our results to cases where transverse hydrodynamical dispersion is controlled by transverse mechanical dispersion and not by molecular diffusion.

[52] In short, the proposed MRMT-R does represent quite accurately upscaled reactive transport through heterogeneous media using solely data derived from conservative transport. We attribute this behavior to the fact that the MRMT model allows approximating the distribution of concentrations (that is, the actual PDF is approximated by the distribution of mobile and immobile concentrations) and, hence, the nonlinearity of reactions. Still, a note of caution must be made on the practical use of the method. The approach is only valid if the BTC is representative for the individual travel paths. As mentioned in the introduction, the observed BTC may result from superimposing independent flow paths with little mixing. In such cases, which should be expected in plumes or if injection only spans a portion of the aquifer thickness, the approach would overestimate mixing and reaction. A detailed accounting of geological heterogeneity or, perhaps, a nonlocal in space approach would be required in those cases.

Appendix A: Some Details on the Numerical Implementation of a Discrete MRMT-R Model

[53] MRMT-R model presented here is implemented in the 2D finite element code TRACONF [*Carrera et al.*, 1989]. The implementation of the general, conservative MRMT scheme was outlined in Appendix A of *Willmann et al.* [2008]. Additionally, after solving transport for the component u, the mass balance for the reaction rate in the mobile zone (equation (15)) and all immobile zones (equation (21)) have to be calculated at each time step. Both are mass balance equations where the unknown is the reaction rate. Generally, the implementation of this reactive mass transfer scheme is straight forwards. Still, two difficulties exist; the treatment of boundary conditions involving explicitly u and solving the problem implicitly.

[54] The boundary conditions have to be corrected for those operations that involve explicit values of u (like for fixed concentration or flux dependent mass inflow). The mass balance in equation (15) only closes if this correction is performed. The respective mathematical operation setting the boundary conditions has to be reverted and performed again with c_2 replacing u. For solving transport at an implicit scheme it is critical to set the time correctly for the weighting of u and c_2. One can either calculate the reaction rate at time $k + \theta$ or the reaction rates at times k and $k + 1$ are weighted by θ and $1 - \theta$ respectively. We found much lower mass balance error for the latter case.

Appendix B: Derivation of Equation (5)

[55] We start from equation (2) written in Laplace space

$$\widetilde{\Gamma}_j = \phi_{i_{tot}} \widetilde{g}(s\widetilde{c}_{m,j} - c_{m0,j}) \tag{B1}$$

From (3), it immediately follows that

$$\widetilde{g} = \sum_{i=1}^{N} \frac{\alpha_i b_i}{\alpha_i + s} \tag{B2}$$

also, from equation (4) it directly follows that

$$s\widetilde{c}_{im,j,i} - c_{im0,j,i} = \alpha_i \widetilde{c}_{m,j} - \alpha_i \widetilde{c}_{im,j,i} \tag{B3}$$

with the subindex 0 indicating initial values. Isolating $\widetilde{c}_{m,j}$ in equation (18) and substituting it together with equations (B2) and (B1) we obtain

$$\widetilde{\Gamma}_j = \sum_{i=1}^{N} b_i \phi_{i_{tot}} \left(\alpha_i (\widetilde{c}_{m,j} - \widetilde{c}_{im,j,i}) - \frac{\alpha_i}{\alpha_i + s} (c_{m0,j} - c_{im0,j,i}) \right) \tag{B4}$$

if initially the system was in equilibrium regarding the mobile and immobile phases, the last term in equation (B4) cancels out and by taking the inverse Laplace transform of the resulting equation we immediately recover equation (5).

[56] **Acknowledgments.** This work was partly funded by ENRESA and the European Commission through the project FUNMIG and by the Spanish agency for scientific research (CICYT) through project CTM2007-66724. The first author acknowledges additional financial support by Agència de Gestió d'Ajuts Universitaris i de Recerca (AGAUR) of the Catalan Regional Government. We also want to acknowledge the input by the persons involved in the very constructive review process, the three reviewers (Olaf Cirpka, David Benson, and an anonymous one), the associate editor (Alberto Bellin), and the managing editor (Brian Berkowitz). Their detailed comments and positive criticism helped us to substantially improve our paper.

References

Adams, E. E., and L. W. Gelhar (1992), Field study of dispersion in a heterogeneous aquifer: 2. Spatial moment analysis, *Water Resour. Res.*, *28*(12), 3293–3308.

Bellin, A., A. Rinaldo, W. J. P. Bosma, S. E. A. T. M. van der Zee, and Y. Rubin (1993), Linear equilibrium adsorbing solute transport in physically and chemically heterogeneous porous formations: 1. Analytical solutions, *Water Resour. Res.*, *29*(12), 4019–4030.

Benson, D. A., S. W. Wheatcraft, and M. M. Meerschaerdt (2000), The fractional-order governing equation of Lévy motion, *Water Resour. Res.*, *36*(6), 1413–1423, doi:10.1029/2000WR900032.

Berkowitz, B., and H. Scher (1998), Theory of anomalous chemical transport in fracture networks, *Phys. Rev. E*, *57*(5), 5858–5869.

Berkowitz, B., A. Cortis, M. Dentz, and H. Scher (2006), Modeling non-Fickian transport in geological formations as a continuous time random walk, *Rev. Geophys.*, *44*, RG2003, doi:10.1029/2005RG000178.

Berkowitz, B., S. Emmanuel, and H. Scher (2008), Non-Fickian transport and multiple-rate mass transfer in porous media, *Water Resour. Res.*, *44*, W03402, doi:10.1029/2007WR005906.

Binning, P. J., and M. A. Celia (2008), Pseudokinetics arising from the upscaling of geochemical equilibrium, *Water Resour. Res.*, *44*, W07410, doi:10.1029/2007WR006147.

Carrera, J. (1993), An overview of uncertainties in modelling groundwater solute transport, *J. Contam. Hydrol.*, *13*(1–4), 23–48, doi:10.1016/0169-7722(93)90049-X.

Carrera, J., G. Galarza, and A. Medina (1989), *TRACONF: User's Guide*, Tech. Univ. of Catalonia, Barcelona, Spain.

Carrera, J., X. Sánchez-Vila, I. Benet, A. Medina, G. Galarza, and J. Guimera (1998), On matrix diffusion: Formulations, solution methods and qualitative effects, *Hydrogeol. J.*, *6*(1), 178–190, doi:10.1007/s100400050143.

Cirpka, O. A., and P. K. Kitanidis (2000), Characterization of mixing and dilution in heterogeneous aquifers by means of local temporal moments, *Water Resour. Res.*, *36*(5), 1221–1236.

Cirpka, O. A., R. Schwede, J. Luo, and M. Dentz (2008), Concentration statistics of reactive constitutents in random hetrogeneous media, *J. Contam. Hydrol.*, *98*, 61–74.

Cortis, A., and B. Berkowitz (2004), Anomalous transport in "classical" soil and sand columns, *Soil Sci. Soc. Am. J.*, *68*, 1539–1548.

Dagan, G. (1989), *Flow and Transport in Porous Formations*, 465 pp., Springer, Berlin.

De Simoni, M., J. Carrera, X. Sánchez-Vila, and A. Guadagnini (2005), A procedure for the solution of multicomponent reactive transport problems, *Water Resour. Res.*, *41*, W11410, doi:10.1029/2005WR004056.

De Simoni, M., X. Sánchez-Vila, J. Carrera, and M. Saaltink (2007), A mixing ratios-based formulation for multicomponent reactive transport, *Water Resour. Res.*, *43*, W07419, doi:10.1029/2006WR005256.

Dentz, M., and B. Berkowitz (2003), Transport behavior of a passive solute in continuous time random walks and multirate mass transfer, *Water Resour. Res.*, *39*(5), 1111, doi:10.1029/2001WR001163.

Dentz, M., and B. Berkowitz (2005), Exact effective transport dynamics in a one-dimensional random environment, *Phys. Rev. E*, *72*(3), 031110.

Dentz, M., and J. Carrera (2007), Mixing and spreading in stratified flow, *Phys. Fluids*, *19*, 017107, doi:10.1063/1.2427089.

Dentz, M., and A. Castro (2009), Effective transport dynamics in porous media with heterogeneous retardation properties, *Geophys. Res. Lett.*, *36*, L03403, doi:10.1029/2008GL036846.

Dentz, M., H. Kinzelbach, S. Attinger, and W. Kinzelbach (2000), Temporal behavior of a solute cloud in a heterogeneous porous medium: 1. Point-like injection, *Water Resour. Res.*, *36*(12), 3591–3604.

Dentz, M., A. Cortis, H. Scher, and B. Berkowitz (2004), Time behavior of solute transport in heterogeneous media: Transition from anomalous to normal transport, *Adv. Water Resour.*, *27*, 155–173.

Donado, L. D., X. Sanchez-Vila, M. Dentz, J. Carrera, and D. Bolster (2009), Multicomponent reactive transport in multicontinuum media, *Water Resour. Res.*, *45*, W11402, doi:10.1029/2008WR006823.

Fernandez-Garcia, D., X. Sánchez-Vila, and A. Guadagnini (2008), Reaction rates and effective parameters in stratified aquifers, *Adv. Water Resour.*, *31*(10), 1364–1376, doi:10.1016/j.advwatres.2008.07.001.

Gelhar, L. (1993), *Stochstic Subsurface Hydrology*, Prentice Hall, Old Tappan, New York.

Gómez-Hernández, J., and A. Journel (1993), Joint sequential simulation of multigaussian fields, in *Geostat Troia 1992*, vol. 1, edited by A. Soares, pp. 85–94, Kluwer, Dordrecht, Netherlands.

Haggerty, R., and S. M. Gorelick (1995), Multiple-rate mass transfer for modeling diffusion and surface reactions in media with pore scale heterogeneity, *Water Resour. Res.*, *31*(10), 2383–2400.

Haggerty, R., and S. M. Gorelick (1998), Modeling mass transfer processes in soil columns with pore-scale heterogeneity, *Soil Sci. Soc. Am. J.*, *62*(1), 62–74.

Haggerty, R., S. A. McKenna, and L. C. Meigs (2000), On the late-time behavior of tracer test breakthrough curves, *Water Resour. Res.*, *36*(12), 3467–3479.

Haggerty, R., C. F. Harvey, C. Freiherr von Schwerin, and L. C. Meigs (2004), What controls the apparent timescale of solute mass transfer in aquifers and soils? A comparison of experimental results, *Water Resour. Res.*, *40*, W01510, doi:10.1029/2002WR001716.

Kapoor, V., and P. K. Kitanidis (1998), Concentration fluctuations and dilution in aquifers, *Water Resour. Res.*, *34*(5), 1181–1193.

Kitanidis, P. K. (1988), Prediction by the method of moments of transport in a heterogeneous formation, *J. Hydrol.*, *102*, 453–473.

Kitanidis, P. K. (1994), The concept of the dilution index, *Water Resour. Res.*, *30*(7), 2011–2026.

Knudby, C., and J. Carrera (2006), On the use of apparent hydraulic diffusivity as an indicator of connectivity, *J. Hydrol.*, *329*(3–4), 377–389, doi:10.1016/j.jhydrol.2006.02.026.

Kosakowski, G., B. Berkowitz, and H. Scher (2001), Analysis of field observations of tracer transport in a fractured till, *J. Contam. Hydrol.*, *47*(1), 29–51.

Lawrence, A. E., X. Sanchez-Vila, and Y. Rubin (2002), Conditional moments of the breakthrough curves of kinetically sorbing solute in heterogeneous porous media using multirate mass transfer models for sorption and desorption, *Water Resour. Res.*, *38*(11), 1248, doi:10.1029/2001WR001006.

Le Borgne, T., and P. Gouze (2008), Non-Fickian dispersion in porous media: 2. Model validation from measurements at different scales, *Water Resour. Res.*, *44*, W06427, doi:10.1029/2007WR006279.

Levy, M., and B. Berkowitz (2003), Measurement and analysis of non-Fickian dispersion in heterogeneous porous media, *J. Contam. Hydrol.*, *64*(3–4), 203–226.

Lichtner, P. C., and Q. Kang (2007), Upscaling pore-scale reactive transport equations using a multiscale continuum formulation, *Water Resour. Res.*, *43*, W12S15, doi:10.1029/2006WR005664.

Luo, J., and O. A. Cirpka (2008), Traveltime-based descriptions of transport and mixing in heterogeneous domains, *Water Resour. Res.*, *44*, W09407, doi:10.1029/2007WR006035.

Luo, J., M. Dentz, J. Carrera, and P. Kitanidis (2008), Effective reaction parameters for mixing controlled reactions in heterogeneous media, *Water Resour. Res.*, *44*, W02416, doi:10.1029/2006WR005658.

Margolin, G., M. Dentz, and B. Berkowitz (2003), Continuous time random walk and multirate mass transfer modeling of sorption, *Chem. Phys.*, *295*, 71–80.

McKenna, S., L. Meigs, and R. Haggerty (2001), Tracer tests in a fractured dolomite: 3. Double porosity, multiple-rate mass-transfer processes in two-well convergent flow tests, *Water Resour. Res.*, *35*(7), 1143–1154.

Medina, A., and J. Carrera (1996), Coupled estimation of flow and solute transport parameters, *Water Resour. Res.*, *32*(10), 3063–3076.

Neuman, S. P. (1990), Universal scaling of hydraulic conductivities and dispersivities in geologic media, *Water Resour. Res.*, *22*(8), 1749–1758.

Neuman, S., and D. Tartakovsky (2009), Perspective on theories of anomaloustransport in heterogeneous media, *Adv. Water Resour.*, *32*(5), 670–680, doi:10.1016/j.advwatres.2008.08.005.

Rezaei, M., E. Sanz, E. Raeisi, E. Vázquez-Suñé, C. Ayora, and J. Carrera (2005), Reactive transport modeling of calcite dissolution in the fresh-salt water mixing zone, *J. Hydrol.*, *311*, 282–298.

Riva, M., and M. Willmann (2009), Impact of log-transmissivity variogram structure on groundwater flow and transport predictions, *Adv. Water Resour.*, *32*, 1311–1322, doi:10.1016/j.advwatres.2009.05.007.

Roth, K., and W. A. Jury (1993), Linear transport models for adsorbing solutes, *Water Resour. Res.*, *29*(4), 1195–1203.

Rubin, Y. (1983), Transport of reactive solute in porous media: Relation between mathematical nature of problem formulation and chemical nature of reactions, *Water Resour. Res.*, *19*(5), 1231—1252.

Rubin, Y., M. A. Cushey, and A. Wilson (1997), The moments of the breakthrough curves of instantaneously and kinetically sorbing solutes in heterogeneous geologic media: Prediction and parameter inference from field measurements, *Water Resour. Res.*, *33*(11), 2465–2481.

Sánchez-Vila, X., I. Colominas, and J. Carrera (1993), *FAITH: User's Guide*, Tech. Univ. of Catalonia, Barcelona, Spain.

Schumer, R., D. A. Benson, M. M. Meerschaert, and B. Baeumer (2003), Fractal mobile/immobile solute transport, *Water Resour. Res.*, *39*(10), 1296, doi:10.1029/2003WR002141.

Selroos, J. O., and V. Cvetkovic (1992), Modeling solute advection coupled with sorption kinetics in heterogeneous formations, *Water Resour. Res.*, *28*(5), 1271–1278.

Silva, O., J. Carrera, S. Kumar, M. Dentz, A. Alcolea, and M. Willmann (2009), A general real-time formulation for multi-rate mass transfer problems, *Hydrol. Earth Syst. Sci.*, *13*(8), 1399–1411.

Valocchi, A. J. (1985), Validity of the local equilibrium assumption for modeling sorbing solute transport through homogeneous soils, *Water Resour. Res.*, *21*(6), 808–820.

Werth, C. J., O. A. Cirpka, and P. Grathwohl (2006), Enhanced mixing and reaction through flow focusing in heterogeneous porous media, *Water Resour. Res.*, *42*, W12414, doi:10.1029/2005WR004511.

Willmann, M., J. Carrera, and X. Sánchez-Vila (2008), Transport upscaling in heterogeneous aquifers: What physical parameters control memory functions?, *Water Resour. Res.*, *44*, W12437, doi:10.1029/2007WR006531.

Zavala-Sanchez, V., M. Dentz, and X. Sanchez-Vila (2009), Characterization of mixing and spreading in a bounded stratified medium, *Adv. Water Resour.*, *32*, 635—648.

Zhang, Y., D. A. Benson, and B. Baeumer (2007), Predicting the tails of breakthrough curves in regional-scale alluvial systems, *Ground Water*, *45*(4), 473–484, doi:10.1111/j.1745-6584.2007.00320.x.

Zinn, B., L. C. Meigs, C. F. Harvey, R. Haggerty, W. J. Peplinski, and C. F. von Schwerin (2004), Experimental visualization of solute transport

and mass transfer processes in two-dimensional conductivity fields with connected regions of high conductivity, *Environ. Sci. Technol.*, *38*(14), 3916–3926, doi:10.1021/es034958g.

J. Carrera, M. Dentz, and O. Silva, Institute of Environmental Assessment and Water Research, CSIC, Lluis Sole i Sabaris s/n, E-08028, Barcelona, Spain.

X. Sanchez-Vila, Department of Geotechnical Engineering and Geosciences, Technical University of Catalonia, Jordi Girona 31, E-08034 Barcelona, Spain.

M. Willmann, Institute of Environmental Engineering, ETH Zurich, HIL G 31.3, Wolfgang-Pauli-Str. 15, CH-8093 Zurich, Switzerland. (willmann@ifu.baug.ethz.ch)